

A Social Force Based Pedestrian Motion Model Considering Multi-Pedestrian Interaction with a Vehicle

DONGFANG YANG, ÜMIT ÖZGÜNER, and KEITH REDMILL, The Ohio State University

Pedestrian motion modeling in mixed traffic scenarios is crucial to the development of autonomous systems in transportation related applications. This work investigated how pedestrian motion is affected by surrounding pedestrians and vehicles, i.e., vehicle-pedestrian interaction. A social force based pedestrian motion model was proposed, in which the effect of surrounding pedestrians was improved and the effect of vehicles was newly designed. Variable constraints dependent on vehicle influence as well as nearby pedestrian density were imposed on the velocity and acceleration of the pedestrian motion. This work focuses on fundamental patterns of multi-pedestrian interaction with a low speed vehicle (front, back, and lateral interaction in open space). In other words, the application of the model is not restricted to specific scenarios such as crosswalks. Parameters of the proposed model were calibrated by the genetic algorithm (GA) based on trajectory data of the same vehicle-pedestrian interaction patterns from controlled experiments. The proposed model is able to simulate complex self-designed vehicle-pedestrian interaction scenarios. The effectiveness of the proposed model was validated by comparing the simulated trajectories with ground truth trajectories under the same initial conditions, and by evaluating the pedestrian behavior of avoiding vehicle in the simulation of self-designed scenarios.

CCS Concepts: • **Networks** → *Traffic engineering algorithms*; • **Theory of computation** → *Genetic programming*; • **Applied computing** → *Transportation*;

Additional Key Words and Phrases: Pedestrian motion, vehicle-pedestrian interaction, social force, genetic algorithm

ACM Reference format:

Dongfang Yang, Ümit Özgüner, and Keith Redmill. 2020. A Social Force Based Pedestrian Motion Model Considering Multi-Pedestrian Interaction with a Vehicle. *ACM Trans. Spatial Algorithms Syst.* 6, 2, Article 11 (February 2020), 27 pages.

<https://doi.org/10.1145/3373646>

1 INTRODUCTION

Pedestrian behavior plays a crucial role in urban mobility. In complex urban scenarios, pedestrian behavior is affected by various types of traffic participants, of which in most cases are surrounding pedestrians and vehicles. Vehicles are usually regarded as the most dominating participants, which

Material reported here was partially supported by the NSF under the CPS Program (awards 1528489 and 1446735) and partially by the U.S. Department of Transportation under award number 69A3551747111 for the Mobility21 University Transportation Center. Any opinions, findings, conclusions, or recommendations expressed herein are those of the authors and do not necessarily reflect the views of the U.S. Department of Transportation or Carnegie Mellon University.

Authors' address: D. Yang, Ü. Özgüner, and K. Redmill, the Ohio State University, 281 West Lane Avenue, Columbus, OH 43210; emails: {yang.3455, ozguner.1, redmill.1}@osu.edu.

Permission to make digital or hard copies of all or part of this work for personal or classroom use is granted without fee provided that copies are not made or distributed for profit or commercial advantage and that copies bear this notice and the full citation on the first page. Copyrights for components of this work owned by others than ACM must be honored. Abstracting with credit is permitted. To copy otherwise, or republish, to post on servers or to redistribute to lists, requires prior specific permission and/or a fee. Request permissions from permissions@acm.org.

© 2020 Association for Computing Machinery.

2374-0353/2020/02-ART11 \$15.00

<https://doi.org/10.1145/3373646>

have considerable influence on pedestrian behavior and even threaten the safety of pedestrians in extreme situation. In the meantime, pedestrian behavior is also affected by surrounding pedestrians. For example, multiple pedestrians may feel more confident than an individual pedestrian when interacting with a vehicle. This work focuses on pedestrian motion, which is the most direct form of pedestrian behavior. The pedestrian motion is described by a social force based mathematical model. The model primarily addresses how the pedestrian motion is affected by surrounding pedestrians and vehicles. With the model applied on each pedestrian, the interaction between multiple pedestrians and a vehicle is described. Typical real traffic scenarios include shared spaces or crowded streets of special events. In such scenarios, both pedestrians and vehicles have equal rights of the road/space, hence not being restricted by specific traffic rules.

The mathematical modeling of pedestrian motion began with pedestrian-pedestrian interaction—for instance, only the effect from surrounding pedestrians is considered. The pioneer work was the social force model [12], which was originally designed for crowd motion/flow simulation and analysis. It can reproduce typical crowd motion patterns such as lane formation and fluctuation, as summarized in a work reviewing fundamental phenomena of pedestrian crowd [27]. Later on, mathematical modelings such as dynamic programming [13], discrete choice [2], cognitive method [22], linear trajectory avoidance [25], and heuristic with Voronoi diagram [30] were proposed. They were somehow derived from the social force model but with more emphasis on computational efficiency and simplicity. These models rely on verified handcrafted mathematical rules to describe the interaction. In addition to the preceding rule-based models, neural network models that build on long short-term memory (LSTM) [1, 9, 31] have recently become an alternative choice of modeling pedestrian motion. Although the application of neural network models is more about motion prediction than simulation, essentially both rule-based models and neural network models share the same feature of addressing pedestrian trajectory.

Now, with vehicle considered, the effect of a vehicle should be somehow incorporated into the pure pedestrian motion models. Some works proposed the modeling of vehicle influence on individual pedestrians [7, 8, 29]. They did not specifically consider multi-pedestrian interaction with vehicles (i.e., the effect of surrounding pedestrians was usually neglected), and the scenarios were usually restricted to crosswalks. The general vehicle-pedestrian interaction is more complicated than the interaction in restricted scenarios. The social force model is one of the options that can easily incorporate the effect of a vehicle. This is because in the social force model, a pedestrian is regarded as a point mass agent, and dynamics of the agent are subject to a summation of individual effects from different sources (e.g., attraction to the destination, repulsion to surrounding pedestrians). The effect of a vehicle can be designed as an additional source into the summation, which is straightforward and effective. Therefore, this work developed multi-pedestrian interaction with a vehicle based on the social force model.

The social force model has been continually improved and modified since its introduction in Helbing and Molnar [12]. The original model only considered the repulsion and attraction of surrounding pedestrians, as well as the attraction of the destination. Later on, collision force was added to account for extremely crowded situations such as emergency evacuation or pilgrimage [11]. In Zanlungo et al. [34], the authors summarized and compared different specifications of the effect of surrounding pedestrians. To more accurately describe the effect of surrounding pedestrians, realistic pedestrian trajectory data [17, 25] was utilized to calibrate the parameters of the social force model. Most calibration approaches adopted the genetic algorithm (GA) [13, 14, 34], evaluated based on the difference between the ground truth trajectories and simulated trajectories of the social force model.

Different approaches have been attempted to add vehicle influence into the social force model. Some works [3, 33, 35, 36] modeled the vehicle influence as an additional force added on the

pedestrian dynamics. The additional force not only considered the relative positions and velocities of the vehicle, as in the effect of surrounding pedestrians, but also other vehicle features such as size, shape, and restriction on motion were considered. To address the complexity introduced by vehicle influence, multi-layer models that contain social force were proposed [3, 15, 24, 26, 28, 35]. Social force was embedded into a layer usually referred to as behavioral layer. Above the behavioral layer, there is another layer mainly responsible for finding a global route or intermediate destinations that can guide the pedestrian motion. The social force of the behavioral layer is only responsible for adjusting local motion. For example, in Schönauer et al. [28], the proposed model consists of three different layers that are primarily responsible for scene context effect, local motion of the agents, and road conflicts, respectively. Vehicle influence does not only exist in the layer of social force but also part of the influence is described in other layers in combination with specific approaches, such as conflict resolving via the “shadow” method in Anvari et al. [3], game theory in Johora and Müller [15] and Schönauer et al. [28], and long range and short range conflicts in Pascucci et al. [24] and Rinke et al. [26].

This work, however, applies a single-layer social force model. Instead of accounting for the complexity introduced by the interaction of different types of road users, the proposed model focuses on the effect of the vehicle itself inside the social force model. Moreover, the model aims to describe fundamental interaction scenarios of multi-pedestrian interaction with a vehicle, and hence the model does not consider any scene information, which is the main reason and the basis for applying multi-layer models.

The proposed social force model mathematically describes the pedestrian motion that is primarily affected by multiple surrounding pedestrians and a low-speed vehicle. The model introduced a general vehicle-pedestrian interaction design that was validated by fundamental interaction scenarios of multiple pedestrians coming from different directions and interacting with the vehicle (front, back, and lateral interaction). Our main contributions are summarized as follows:

- We summarized and analyzed fundamental elements (decaying functions, anisotropies) that were frequently and repeatedly used in the social force model.
- We modified the effect of surrounding pedestrians in the social force model based on several existing works.
- The effect of the vehicle was newly designed so that it had a similar format of the effect of surrounding pedestrians. The effect considered the size, shape, and longitudinal velocity of the vehicle.
- We introduced variable constraints on the limits of pedestrian velocity and acceleration that are dependent on the magnitude of vehicle influence and the density of nearby pedestrians.
- We applied the genetic algorithm (GA) to calibrate the proposed model. The calibration was accomplished based on pedestrian trajectory data of a high frame rate (30 frames per second). The calibrated model was validated based on the reproduction of fundamental interaction scenarios in simulation.

2 PROBLEM FORMULATION

The fundamental problem is to design a social force based mathematical model that describes pedestrian motion in mixed traffic scenarios, primarily considering the effect of surrounding pedestrians and vehicles. The model should be able to generate future motion of the ego pedestrian based on the immediate status of the pedestrian. In other words, given the current states of all interacting agents (positions and velocities of all surrounding pedestrians and vehicles), the associated model should output the next step’s position and velocity of the ego pedestrian. With each individual pedestrian assigned with a model, trajectories of all pedestrians can be generated

by iteratively applying the models. The generated trajectories are also referred to as the predicted motion of the pedestrians.

Since multi-pedestrian interaction with a low-speed vehicle is primarily considered in this work, the interaction scenarios are defined such that there are at least five pedestrians and the vehicle speed should be less than 4 m/s. The pedestrian number and the vehicle speed were empirically determined, which may vary in other circumstances. Multiple pedestrians are also referred to as crowd in this work. The low-speed vehicle applies in most shared space scenarios, in which pedestrians and vehicles are mixed together to share the right of the road/space and the vehicle usually pays more attention to the pedestrians. The space layout is assumed to be empty, hence no scene information. This configuration releases the vehicle from being restricted in lanes so that a variety of vehicle maneuvers are available.

Mathematically, if we define, at time t , the state (position and velocity) of pedestrian i as $\vec{x}_t^i = (x_t^i, y_t^i, v_{x,t}^i, v_{y,t}^i)^T$, the state (position, speed, and orientation) of vehicle as \vec{x}_t^v , the model can be expressed as follows:

$$\vec{x}_{t+1}^i = f_i(\vec{x}_t^i, \{\vec{x}_t^{j \neq i}\}, \vec{x}_t^v). \quad (1)$$

This work does not focus on the generation of vehicle motion, and hence the vehicle state $\{\vec{x}_t^v, \forall t\}$ is assumed to be known all the time. It is either directly obtained from the trajectory dataset or intentionally synthesized. When intentionally synthesized, a kinematic bicycle model with a pure pursuit steering controller and a PID speed controller is applied to generate more realistic vehicle motion.

3 PEDESTRIAN MOTION MODELING

3.1 Fundamental Functions

Some fundamental functions are described in this section, because they serve as essential components in the proposed social force pedestrian motion model. They are anisotropy functions and decaying functions. Anisotropy functions are used to describe the different effect of the interacting agents from different directions. For example, a pedestrian right in front of the ego pedestrian obviously has bigger influence than a pedestrian on the left or right side of the ego pedestrian. Decaying functions are used to describe the different effect of different interaction distances. For example, a vehicle that is very far away from the ego pedestrian has merely no influence, whereas a vehicle that is very close to the ego pedestrian surely has large influence. Both types of functions have different specifications, which are selected based on the specific requirement of each component of the model.

3.1.1 Anisotropy Functions. Anisotropy functions take input as the angle between the ego pedestrian's walking direction and the direction to the target agent that is interacting with the ego pedestrian. The output of anisotropy function is a scalar ranging from 0 to 1, representing how the influence attenuates as the angle increases.

Three different types of anisotropies (linear, sinusoidal, and exponential) are used in this work, as shown in Figure 1, with the following expressions:

$$\mathbb{A}_{lin}(\phi, \lambda) = \max \left\{ 1 - \lambda \cdot \frac{|\phi|}{\pi}, 0 \right\}, \quad (2)$$

$$\mathbb{A}_{sin}(\phi, \lambda) = \lambda + (1 - \lambda) \cdot \frac{1 + \cos |\phi|}{2}, \quad (3)$$

$$\mathbb{A}_{exp}(\phi, \lambda) = \exp(-\lambda \cdot |\phi|), \quad (4)$$

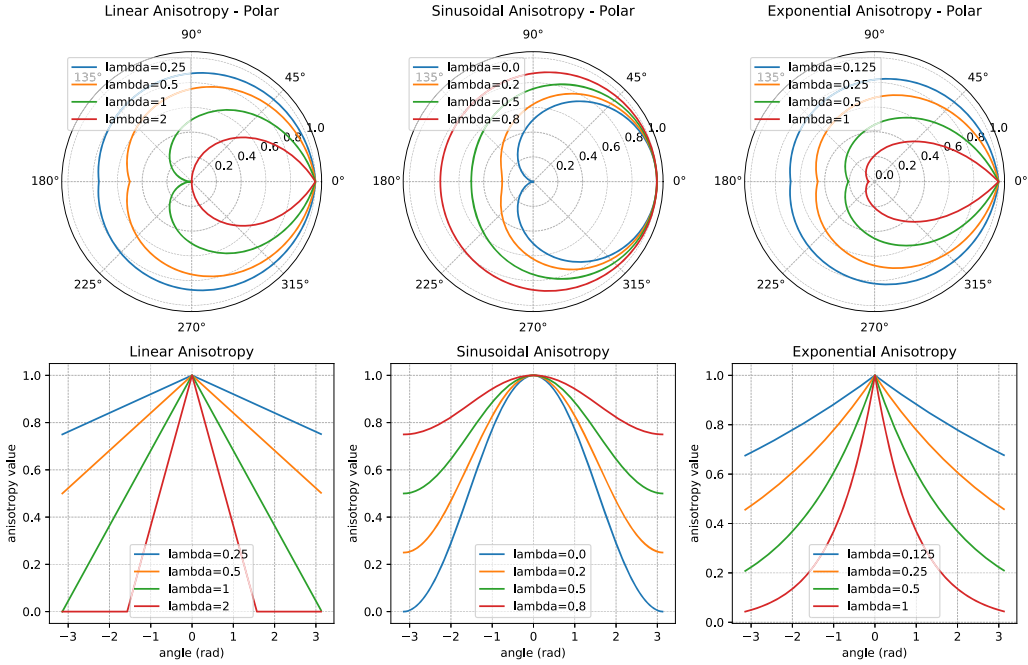


Fig. 1. Illustration of different anisotropies. Columns from left to right: Linear anisotropy, sinusoidal anisotropy, and exponential anisotropy. Different parameter values generate different anisotropies.

where $\phi \in [-\pi, \pi]$ is a variable representing the interaction angle and λ is the parameter adjusting the anisotropy characteristics. The major difference among these anisotropies is the rate of attenuation at the angles near 0. For example, as $|\phi|$ increases from 0 to a certain angle (e.g., 90 degrees), exponential anisotropy attenuates very fast, but sinusoidal anisotropy attenuates relatively slow (see the second row in Figure 1). This difference plays an important role in modeling a pedestrian's reaction to a target agent.

3.1.2 Decaying Functions. Decaying functions take input as the distance between the ego pedestrian to the target agent. The output is the magnitude of the influence (i.e., the force magnitude applied to the point mass dynamics). The magnitude decreases monotonically as the distance increases.

Exponential function, as shown in the left of Figure 2, is a common option in most social force models, due to its simplicity and effectiveness:

$$f_{exp}(d, A, B) = A \exp(-Bd), \quad (5)$$

where d is a variable representing the distance between the ego pedestrian and the target agent, and A, B are parameters adjusting the characteristics of the decaying relationship.

Another type of decaying function, as shown in the middle of Figure 2, describes a linear relationship with smoothness modification [6] on the point where the magnitude reaches zero:

$$f_{lm}(d, d_0, M, \sigma) = \frac{M}{2d_0} \cdot \left(d_0 - d + \sqrt{(d_0 - d)^2 + \sigma} \right), \quad (6)$$

where d is again a variable representing the distance, M is the force magnitude when the distance reaches zero (physical touch happens), σ is the parameter that modifies the smoothness around

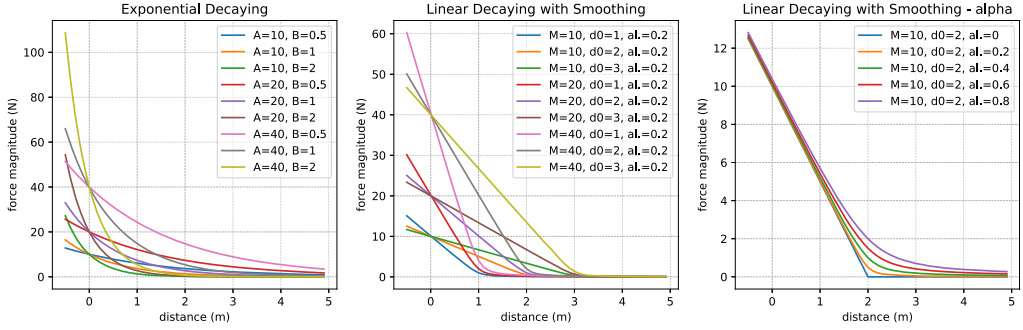


Fig. 2. Illustration of decaying functions. Left: Exponential decaying with different parameter values. Middle: Linear function with smoothing with different parameter values while α is fixed. Right: Linear function with smoothing with different parameter values while M and d_0 are fixed.

zero magnitude, and d_0 is a threshold distance where the magnitude almost reaches zero (equals zero if $\sigma = 0$).

The exponential function is effective in most situations, which has been demonstrated in various social force based models. In an exponential function, the rate of decaying is still exponential, which is helpful in some situations. For example, in the scenario of a vehicle approaching the ego pedestrian, when the distance from the ego pedestrian to the vehicle is very close, the exponential increase of the magnitude of the vehicle influence quickly drives the pedestrian away from the vehicle, which is normal due to the severe consequence of potential collision. However, the exponential relationship can be unrealistic in other situations. For example, the change of effect of a surrounding pedestrian from 4 m to 2 m prefers a more linear relationship than an exponential relationship.

3.2 Pedestrian Dynamics

Pedestrians are regarded as point mass agents in the social force model. The motion of an agent is governed by Newtonian dynamics with the state of position x^i , y^i and velocity v_x^i , v_y^i expressed as follows:

$$\dot{x}^i = v_x^i, \quad (7)$$

$$\dot{y}^i = v_y^i, \quad (8)$$

$$\dot{v}_x^i = a_x^i = \frac{F_x^i}{m^i}, \quad (9)$$

$$\dot{v}_y^i = a_y^i = \frac{F_y^i}{m^i}, \quad (10)$$

where m^i is the mass of pedestrian i and $\vec{F}_t^i = (F_{x,t}^i, F_{y,t}^i)^T$ is the total force applied on the point mass. The preceding dynamics are discretized by a discretization time of Δt in this work. Therefore, a state-space vector $\vec{x}_t^i = (x_t^i, y_t^i, v_{x,t}^i, v_{y,t}^i)^T$ at time t is updated at every timestep after calculating the total force $\vec{F}_t^i = (F_{x,t}^i, F_{y,t}^i)^T$ based on the immediate interaction status.

According to the definition of *social force model*, the total force \vec{F}_t^i is the summation of multi-source effect:

$$\vec{F}_t^i = \vec{F}_t^{i,ped} + \vec{F}_t^{i,veh} + \vec{F}_t^{i,des}, \quad (11)$$

where $\vec{F}_t^{i,ped}$ is the pedestrian-pedestrian interaction force (effect of surrounding pedestrians), $\vec{F}_t^{i,veh}$ the vehicle-pedestrian interaction force (effect of vehicle), and $\vec{F}_t^{i,des}$ the destination force (effect of attraction of destination), all of which are detailed in the following sections.

Although each pedestrian is viewed as a point-mass agent, a virtual radius of R_i is considered when calculating the distance between the ego pedestrian and a target pedestrian. This allows two pedestrians to overlap a little bit with each other, which is regarded as the effect of pushing and squeezing. Therefore, the boundary distance between two pedestrians are defined as follows:

$$d_t^{ij} = |\vec{r}_t^{ij}| - R_i - R_j, \quad (12)$$

where $\vec{r}_t^{ij} := (x_t^j, y_t^j)^T - (x_t^i, y_t^i)^T$ is a vector that points from the ego pedestrian i to the target pedestrian j .

3.3 Constraints

Limits of velocity and acceleration are imposed on pedestrian motion. There is an absolute limit beyond which the pedestrian can never reach due to the physiological limit of human beings. In normal conditions, pedestrians do not reach the limit unless something emergent happens (e.g., a vehicle is approaching in a dangerous way). Pedestrians also tend to restrict the velocities and accelerations within a certain range to walk comfortably in free flow or to adapt particular situations (e.g., when the pedestrian density increases, the pedestrian naturally slows down). Therefore, the constraints applied on both the velocity and the acceleration are time dependent. In this work, the constraints account for the vehicle-pedestrian interaction force $\vec{F}_t^{i,veh}$ and the reciprocal of nearby pedestrian density (i.e., the sparseness of nearby pedestrians S_t^i):

$$|\vec{v}_t^i| \leq v_{lim,t}^i(\vec{F}_t^{i,veh}, S_t^i), \quad (13)$$

$$|\vec{a}_t^i| \leq a_{lim,t}^i(\vec{F}_t^{i,veh}, S_t^i), \quad (14)$$

where

$$S_t^i := \min \left\{ \frac{d_t^{ij}}{\mathbb{A}_{lim}(\phi_t^{ij}, \lambda^S)} \right\}, \forall j \in \mathbb{O}_t^S. \quad (15)$$

$\phi_t^{ij} := \phi_{\langle \vec{v}_t^i, \vec{n}_{ij} \rangle}$ is the angle between the ego pedestrian's walking direction and the direction to the target agent, pedestrian j . λ^S is the anisotropy parameter. \mathbb{O}_t^S defines a fan area centered at the ego pedestrian's walking direction with a radius of threshold T^S and a field of view ϕ^S , which are illustrated in Figure 3(a). The sparseness value of a pedestrian depends on the relative position of the target, as illustrated in Figure 3(b).

In this work, six parameters are defined to model the limits of the velocity and the acceleration. Specifically, they are maximum velocity limit $v_{max} = 2.5$ m/s, normal velocity limit $v_{nor} = 1.7$ m/s, dense velocity limit $v_{den} = 0.3$ m/s, maximum acceleration limit $a_{max} = 5$ m/s², normal acceleration limit $a_{nor} = 2.5$ m/s², and dense acceleration limit $a_{den} = 0.68$ m/s². These values were determined according to the statistical findings in existing studies [4, 18, 19, 21]. Both $v_{lim,t}^i$ and $a_{lim,t}^i$ are designed such that when the sparseness is small, pedestrians are restricted to small velocity and acceleration, but when the vehicle influence is large, the limits increase based on a certain sparseness level. The limits never exceed the maximum values v_{max} and a_{max} . The relationships are expressed as follows:

$$\begin{aligned} v_{lim,t}^i(\vec{F}_t^{i,veh}, S_t^i) &= \min \left(\beta_v^S \cdot \max(S_t^i - S_v^0, 0), v_{nor} - v_{den} \right) + v_{den} \\ &\quad + \min \left(\beta_v^F \cdot \max(|\vec{F}_t^{i,veh}| - F_v^0, 0), v_{max} - v_{nor} \right), \end{aligned} \quad (16)$$

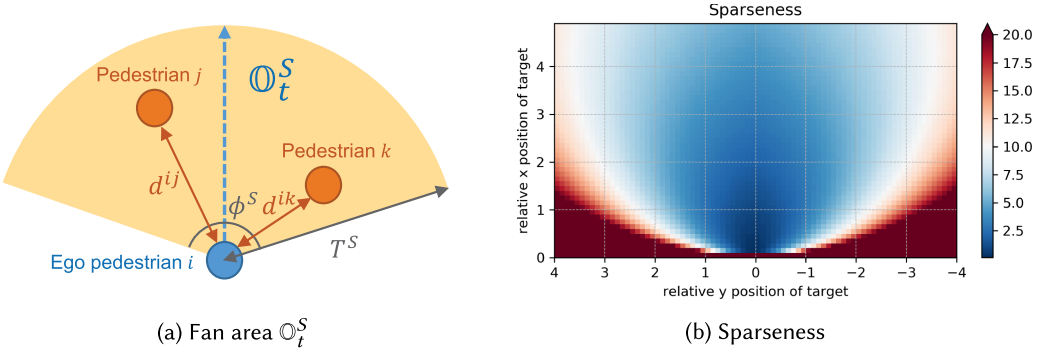


Fig. 3. Sparseness and the corresponding fan area. The sparseness is plotted based on the calibrated parameters shown later in Table 2.

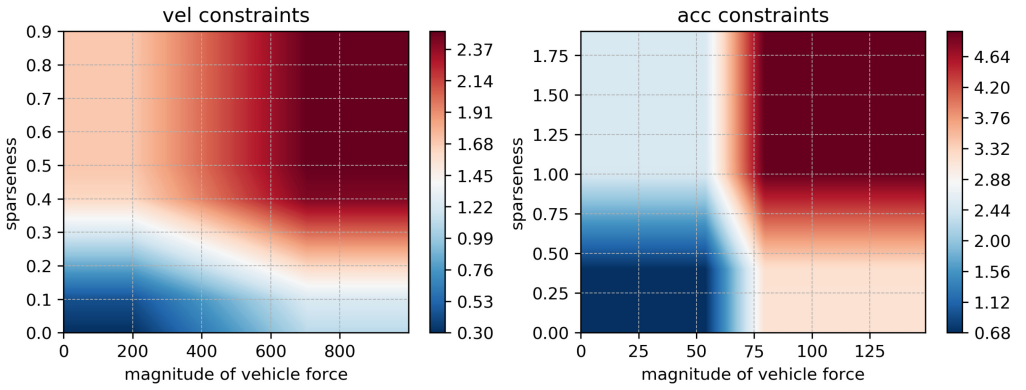


Fig. 4. The constraints on the acceleration and velocity, which are plotted based on the calibrated parameters shown later in Table 2.

$$a_{lim,t}^i(\vec{F}_t^{i,veh}, S_t^i) = \min(\beta_a^S \cdot \max(S_t^i - S_a^0, 0), a_{nor} - a_{den}) + a_{den} \\ + \min(\beta_a^F \cdot \max(|\vec{F}_t^{i,veh}| - F_a^0, 0), a_{max} - a_{nor}), \quad (17)$$

where $\beta_v^S, S_v^0, \beta_v^F, F_v^0, \beta_a^S, S_a^0, \beta_a^F,$ and F_a^0 are parameters that adjust the characteristics of the relationship. Figure 4 provides an example of the constraints on the velocity and the acceleration.

3.4 Pedestrian-Pedestrian Interaction

The pedestrian-pedestrian interaction force accounts for all surrounding pedestrians. Therefore, for ego pedestrian i , the total interaction force is the summation of every individual interaction force. An individual interaction force is further divided into physical collision force $\vec{F}_t^{ij,col}$ and virtual interaction force $\vec{F}_t^{ij,vir}$:

$$\vec{F}_t^{i,ped} = \sum_{j \in \mathbb{Q}(i)} (\vec{F}_t^{ij,col} + \vec{F}_t^{ij,vir}), \quad (18)$$

where $j \in \mathbb{Q}(i)$ denotes the indexes of surrounding pedestrians that belong to ego pedestrian i .

Table 1. Comparison of Different Specifications of Virtual Interaction Force

| Pedestrian Info. Considered | Position | Abs. Velocity | Rel. Velocity |
|-----------------------------|----------|---------------|---------------|
| Circular Specification | Yes | No | No |
| Elliptical Specification | Yes | Yes | No |
| Collision Avoidance | Yes | Yes | Yes |
| Repulsion & Navigation | Yes | Yes | Yes |

3.4.1 Physical Collision Force. Physical collision force is effective only when the distance between two pedestrians is very close or the physical collision happens. This force allows the ego pedestrian to push the target pedestrian, especially in emergent situations such as a vehicle approaching in a dangerous manner. It also describes extremely crowded situations as studied in Helbing et al. [11]. The collision force is expressed as follows:

$$\vec{F}_t^{ij,col} = -\alpha^{col} \cdot \min\{d_t^{ij}, 0\} \cdot \vec{n}_t^{ij}, \quad (19)$$

where \vec{n}_t^{ij} is the unit vector pointing from ego pedestrian i to target pedestrian j , and α^{col} is the parameter. The collision force is effective when the boundary distance d_t^{ij} is negative.

3.4.2 Virtual Interaction Force. Virtual interaction force makes the ego pedestrian keep a certain “social” distance to the target pedestrian. Existing studies have shown some reasonable specifications of the force (circular specification [12], elliptical specification [14], collision avoidance [34], and repulsion & navigation [6]), as summarized in Table 1. The interaction force is formulated as a repulsion force with the magnitude and direction calculated based on the temporal-spatial relationship between the ego and the target. The major difference among these specifications is the amount of information (position, absolute velocity, and relative velocity) used to calculate interaction force (Table 1). This study follows the specification of repulsion & navigation, in which the decaying function of linear relationship with smoothing is applied instead of the exponential relationship as applied in the first three specifications. The navigation part of the force was re-designed by using the fundamental functions.

Therefore, the virtual interaction force used in this study can be expressed as follows:

$$\vec{F}_t^{ij,vir} = \vec{F}_t^{ij,rep} + \vec{F}_t^{ij,nav}, \quad (20)$$

where

$$\vec{F}_t^{ij,rep} = -f_{lm}(d_t^{ij}, d_0^{rep}, M^{rep}, \sigma^{rep}) \cdot \mathbb{A}_{sin}(\phi_t^{ij}, \lambda^{rep}) \cdot \vec{n}_t^{ij}, \quad (21)$$

$$\vec{F}_t^{ij,nav} = f_{lm}(d_t^{ij}, d_0^{nav}, M^{nav}, \sigma^{nav}) \cdot \mathbb{A}_{exp}(\phi_{v,t}^{ij}, \lambda^{nav}) \cdot \vec{n}_{\perp,t}^{ij}. \quad (22)$$

As illustrated in Figure 5, $\phi_{v,t}^{ij} := \phi_{<\vec{v}_t^i, \vec{n}_t^{ij}>}$ is the angle between the direction from ego pedestrian to the target pedestrian, \vec{n}_t^{ij} , and the direction of the relative velocity from pedestrian i to pedestrian j (in terms of pedestrian j 's coordinate), $\vec{v}_t^j = \vec{v}_t^i - \vec{v}_t^j$. The unit vector $\vec{n}_{\perp,t}^{ij}$ is perpendicular to \vec{n}_t^{ij} . Here $\vec{n}_{\perp,t}^{ij}$ has two options (left or right side), depending on which side the $\phi_{v,t}^{ij}$ is.

The repulsion force purely considers the distance between the ego pedestrian and the target pedestrian, which can be interpreted as a social rule of giving enough personal space when walking in a crowd. The linear decaying function with smoothing is applied with the assumption that the repulsion force is more of a linear relationship.

The navigation force is primarily designed for anticipating and avoiding potential collision. It considers both the positions and the velocities of two interacting pedestrians. The navigation is

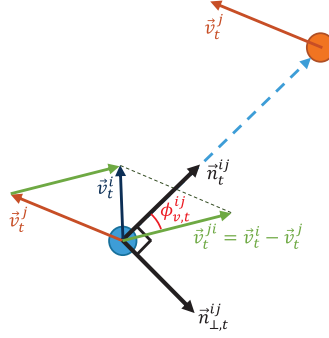


Fig. 5. Illustration of navigational force. The blue circle indicates the ego pedestrian, and the red circle indicates the target pedestrian. The relative velocity (in blue color) represents the relative motion from the ego pedestrian to the target pedestrian.

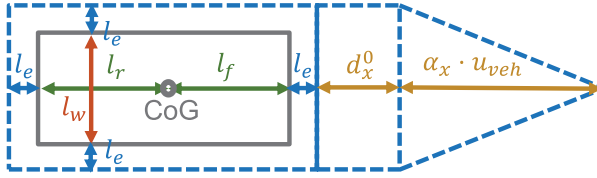


Fig. 6. Vehicle's virtual contour (blue dashed line). A surrounding pedestrian needs to find the influential point (closest point to the virtual contour) and then calculates the vehicle-pedestrian interaction force.

dependent on the relative motion (velocity) between the two interacting pedestrians. If the relative motion indicates that the ego pedestrian is moving toward the target pedestrian ($\phi_{v,t}^{ij}$ is around zero), then a navigation force with the direction of $\vec{n}_{\perp,t}^{ij}$ is generated to avoid the potential collision. The magnitude is calculated based on the distance. An anisotropy is applied to reduce the magnitude when the possibility of collision is becoming small due to a large $\phi_{v,t}^{ij}$.

3.5 Vehicle-Pedestrian Interaction

Vehicle-pedestrian interaction is different from pedestrian-pedestrian interaction, because the collision with a vehicle is strictly not allowed. For the effect of a vehicle as an additional force, existing studies have modeled it as a larger-size pedestrian with elliptical specification [3], pure vehicle shape repulsion [35], and potential-like functions [10, 33]. This work proposes a new design of vehicle-pedestrian interaction force. It considers the spatial-temporal relationship (relative positions and velocities) between the ego pedestrian and the vehicle. The vehicle's size and shape, as well as anisotropy, are also considered. In other words, different pedestrian orientations and velocities and different vehicle orientations of velocities create different combinations of vehicle-pedestrian interaction.

A virtual contour of the vehicle is defined as an extension of the vehicle actual contour and the consequence of slow motion. The virtual contour is illustrated in Figure 6. An extension length l_e is added on based on original contour of the vehicle with length $l_r + l_f$ and width l_w . This can be conceptualized as a minimum distance or a buffer that the ego pedestrian wants to keep from the vehicle. d_x^0 is an extended length along the vehicle's orientation, which assumes that the pedestrian wants to keep a larger distance from the front bumper than from the rear bumper. $\alpha_x \cdot u_{veh}$ is another extended length along a vehicle's moving direction, which is proportional to

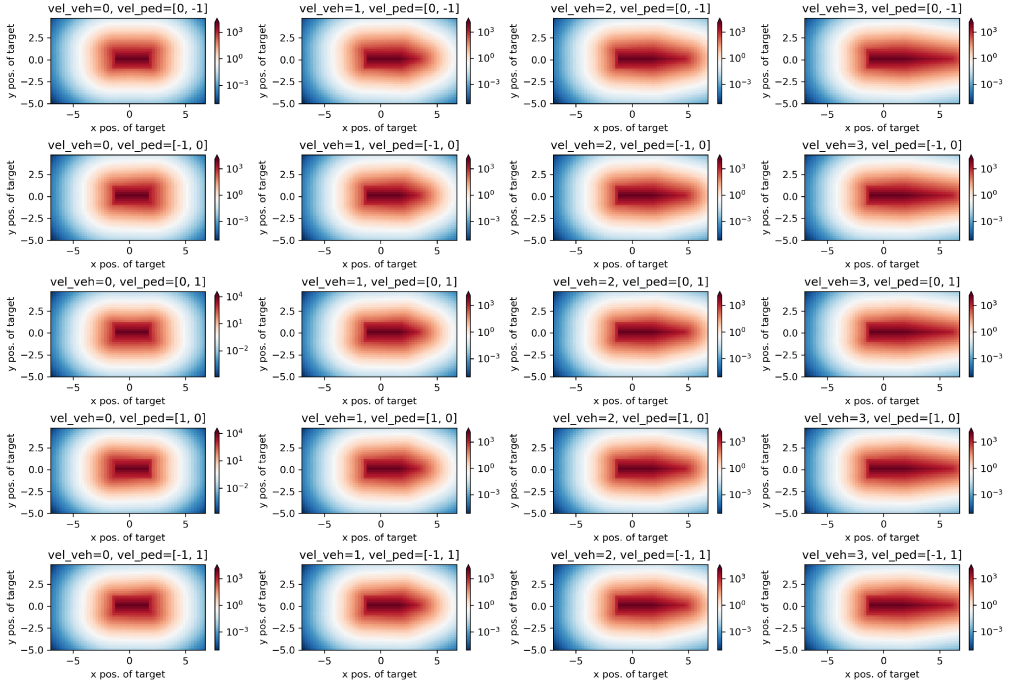


Fig. 7. The magnitudes of vehicle influence under different conditions. Columns from left to right: Vehicle longitudinal speed increases (0 m/s, 1 m/s, 2 m/s, and 3 m/s). Rows from top to bottom: Pedestrian walking direction varies (with velocity vector of $[0, -1]$, $[-1, 0]$, $[0, 1]$, $[1, 0]$, and $[-1, 1]$ in the Euclidean coordinate).

the vehicle longitudinal speed u_{veh} with the parameter α_x . The faster the vehicle, the longer the extension in front of the vehicle.

Once the virtual contour is available, an influential point P_t^{iv} on the contour is determined by finding the minimum distance d_t^{iv} from the ego pedestrian to the contour. Then, the vehicle-pedestrian interaction force is calculated by the following equation:

$$\vec{F}_t^{i,veh} = f_{exp}(d_t^{iv}, A^{veh}, b^{veh}) \cdot \mathbb{A}_{sin}(\phi_t^{iv}, \lambda^{veh}) \cdot \vec{n}_t^{vi}. \quad (23)$$

The direction of the vehicle-pedestrian interaction force is determined by \vec{n}_t^{vi} , which is a unit vector pointing from the influential point to the ego pedestrian. The magnitude applies an exponentially decaying function with parameters A^{veh} and b^{veh} , because as mentioned in the previous section, the pedestrian should be quickly driven away from the vehicle once getting close to the virtual contour. Anisotropy is considered in which $\phi_t^{iv} := \phi_{\langle -\vec{n}_t^{vi}, \vec{v}_t^i \rangle}$ and λ^{veh} is the parameter of the anisotropy. The anisotropy adjusts the magnitude of the vehicle influence based on the walking direction of the pedestrian with respect to the moving direction of the vehicle. For example, a pedestrian walking away from the vehicle should have less vehicle influence than a pedestrian walking toward the vehicle.

Figure 7 presents heat maps that illustrate the magnitudes of vehicle-pedestrian interaction force in different situations. It compares different combinations of longitudinal vehicle speeds and different pedestrian walking directions. As vehicle speed increases, the influence area expands (primarily in the vehicle moving direction). In addition, notice that the difference among the influence areas when the walking direction of the pedestrian changes (different rows).

3.6 Destination Force

Destination force assumes that each pedestrian has a desired walking speed in mind. The pedestrian tries to keep the desired speed as much as possible by generating the destination force:

$$\vec{F}_t^{i,des} = \beta^{des} \cdot k^{des} \cdot (\vec{v}_t^i - \vec{v}_t^{i,d}), \quad (24)$$

where k^{des} is a parameter that can be viewed as feedback gain for the destination force. The desired speed $\vec{v}_t^{i,d}$ is always pointing from the ego pedestrian to the destination and is updated at every timestep:

$$\vec{v}_t^{i,d} = v_0^i \cdot \frac{\vec{x}_t^{i,des} - \vec{x}_t^i}{\sqrt{|\vec{x}_t^{i,des} - \vec{x}_t^i|^2 + (\sigma^{des})^2}}, \quad (25)$$

where the parameter v_0^i represents the desired speed and the parameter σ^{des} reduces the magnitude of desired speed as the pedestrian reaches the destination [6]. $\beta^{des} \in [0, 1]$ in Equation (24) is a function of $|\vec{F}_t^{i,veh}|$ that adjusts the destination force when the effect of vehicle becomes large:

$$\beta^{des} = \max \left\{ \min \left\{ \frac{1}{F_2 - F_1} \cdot (|\vec{F}_t^{i,veh}| - F_2), 1 \right\}, 0 \right\}. \quad (26)$$

It decreases from 1 to 0 with two parameters F_1, F_2 as thresholds. This design allows the pedestrian to switch from reaching the destination to avoiding the collision with vehicle, which is the case in realistic situations.

It is necessary for the destination force to have a destination or temporal goal. In real-time application, it is estimated based on the historical pedestrian trajectory and the scenario layout. If the model is being evaluated based on recorded pedestrian trajectory data, the destination is usually available or can be estimated based on the entire recorded trajectory. If the model is used for the simulation of self-designed scenarios, the destination is usually pre-defined together with the scenario. In this work, the latter two approaches were applied for the model calibration and post-simulation, respectively (see Section 4 and Section 5).

3.7 Vehicle Motion

We believe that vehicles should be considered more as mechanical systems instead of point-mass dynamics similar to pedestrians, because one major purpose of developing the proposed pedestrian motion model is to provide more information for automated systems on vehicles. Specifically, a common procedure (path planning, trajectory generation, and trajectory following) of automated driving is applied. The vehicle motion is generated by a kinematic bicycle model with a pure pursuit path tracking controller that tracks a reference path [16, 23]. The reference paths are usually pre-defined for the simulation of self-designed scenarios. This allows us to test the performance of the proposed pedestrian model in various vehicle-pedestrian interaction patterns. Note that in the process of calibrating model parameters (see Section 4), ground truth vehicle trajectory is directly applied, because the primary focus in this work is pedestrian motion.

4 PARAMETER CALIBRATION

4.1 Parameter Set

All parameters associated with the proposed model are presented in Table 2. They have been classified into three categories:

- *Constant parameters*: The parameters that can be directly assigned based on statistics (e.g., using average pedestrian radius and mass) or ground truth (e.g., vehicle size).

Table 2. List of Calibrated Parameters for the Proposed Model

| Parameter | Calibrated Value | Category |
|-----------------|------------------|-----------------|
| R_i | 0.27 | Constant |
| m_i | 80 | Constant |
| l_r | 1.2 | Constant |
| l_f | 1 | Constant |
| l_w | 1.2 | Constant |
| β_v^S | 3.9761 | Ped2Ped |
| S_v^0 | 0.06566917 | Ped2Ped |
| β_a^S | 2.994062 | Ped2Ped |
| S_a^0 | 0.39941 | Ped2Ped |
| α^{col} | 9825.125 | Ped2Ped |
| d_0^{rep} | 0.7801 | Ped2Ped |
| M^{rep} | 301.028 | Ped2Ped |
| σ^{rep} | 0.45971243 | Ped2Ped |
| λ^{rep} | 0.1 | Ped2Ped (fixed) |
| d_0^{nav} | 1.5892008 | Ped2Ped |
| M^{nav} | 410.875 | Ped2Ped |
| σ^{nav} | 0.41745 | Ped2Ped |
| λ^{nav} | 1 | Ped2Ped (fixed) |
| T^S | 3.665375 | Ped2Ped |
| ϕ^S | 121.39191 | Ped2Ped |
| λ^S | 1.87 | Ped2Ped |
| v_0^i | 1.394293 | Ped2Ped |
| σ^{des} | 1 | Ped2Ped (fixed) |
| k^{des} | 545.3125 | Ped2Ped |
| β_v^F | 0.001577598 | Veh2Ped |
| F_v^0 | 199.3611 | Veh2Ped |
| β_a^F | 0.09775474 | Veh2Ped |
| F_a^0 | 53.94855 | Veh2Ped |
| l_e | 0.2151011 | Veh2Ped |
| d_x^0 | 0.510985 | Veh2Ped |
| α_x | 1.394358 | Veh2Ped |
| A^{veh} | 777.5852 | Veh2Ped |
| b^{veh} | 2.613755 | Veh2Ped |
| λ^{veh} | 0.3119132 | Veh2Ped |
| F_1 | 199.7455 | Veh2Ped |
| F_2 | 672.6487 | Veh2Ped |

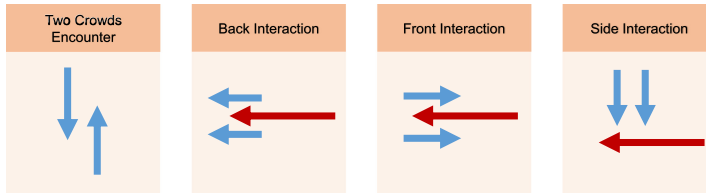


Fig. 8. Scenarios. The first scenario was used for calibrating Ped2Ped parameters, and the following three scenarios were used for calibrating Veh2Ped parameters.

- *Ped2Ped parameters*: The parameters responsible for pedestrian-pedestrian interaction.
- *Veh2Ped parameters*: The parameters responsible for vehicle-pedestrian interaction.

This study applied a two-step procedure for calibrating the parameters. First, the Ped2Ped parameters were calibrated and evaluated based on the trajectory data that does not contain vehicles. In this step, the Veh2Ped parameters were fixed to arbitrary values, because whatever values of the Veh2Ped parameters are set, the vehicle force is always zero. Second, keeping the obtained Ped2Ped parameters fixed, Veh2Ped parameters were then calibrated and evaluated based on the data that contains vehicles. The reason for applying this configuration is that if the Veh2Ped parameters were not fixed in the process of calibrating Veh2Ped parameters, some Ped2Ped parameters might be modified in favor of obtaining better results on the data containing vehicle influence. We argue that the calibration cannot automatically differentiate between Ped2Ped parameters and Veh2Ped parameters.

4.2 Scenarios

Four fundamental scenarios were used for the calibration, as shown in Figure 8. The first scenario was used for pedestrian-pedestrian interaction. After the calibration, the model is expected to generate collective pedestrian behaviors such as lane formation and collision avoidance. Here, only the scenario of bidirectional pedestrian motion is used, because the pedestrian motion patterns are similar in the scenarios that were used for vehicle-pedestrian interaction. The following three scenarios are used for calibrating vehicle-pedestrian interaction. They are fundamental interaction scenarios that consist of back interaction (vehicle coming behind the walking pedestrians), front interaction (vehicle coming in front of the walking pedestrians), and lateral interaction (vehicle coming from both sides of the walking pedestrians).

4.3 Dataset

Trajectories of pedestrians and vehicles that correspond to the scenarios in Figure 8 were collected by conducting controlled experiments. The experiments were conducted at an open space in a parking lot near the CAR-West facility at the Ohio State University, as shown in Figure 9. Pedestrian motion, as well as vehicle motion, were recorded by a drone with a downward camera hovering above the experiment area. To obtain trajectories, positions were extracted by computer vision based tracking techniques, whereas velocities were reconstructed by Kalman filters. There are 80 pedestrian trajectories in total for pedestrian-pedestrian interaction and 96 pedestrian trajectories in total for the vehicle-pedestrian interaction. Details about the dataset can be found in Yang et al. [32].

4.4 Calibration

The calibration consists of manual calibration and data-driven calibration. In the manual calibration, a set of reasonable and acceptable parameters were obtained by trial and error, which was

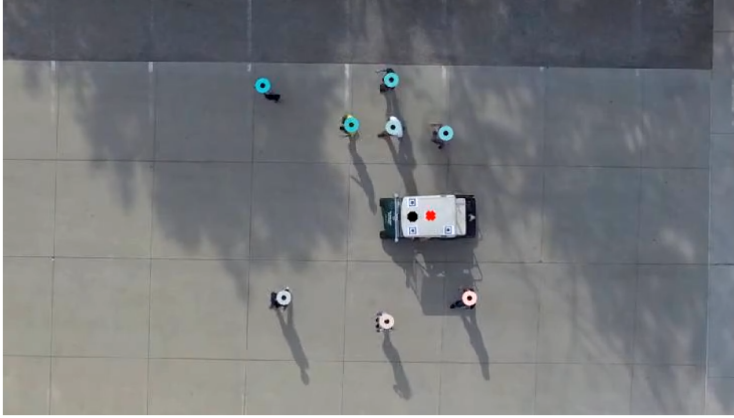


Fig. 9. Illustration of the controlled experiment. Positions of both pedestrians and vehicles were extracted from the top-view video. Velocities were reconstructed by Kalman filters.

evaluated by visually inspecting the simulation results with the obtained parameters. Using the manually calibrated parameters as initial values, the GA was then applied to further calibrate the parameters. The GA calibration was evaluated by the errors between the ground truth trajectories and the simulated trajectories. Ultimately, using the updated parameters, post-simulations were conducted to verify and validate the proposed model.

As mentioned in Section 3.6, a destination is required for the social force model. In the manual calibration, the destinations of all pedestrians were pre-defined in the self-designed scenarios. In the data-driven calibration, a pedestrian's destination was estimated based on the initial position $\vec{x}_0^{i,rec}$ and final position $\vec{x}_T^{i,rec}$ of the recorded trajectory. Specifically, for pedestrian-pedestrian interaction, the destination was estimated individually:

$$\vec{x}_t^{i,des} = \vec{x}_0^{i,rec} + \alpha^{rec} \cdot (\vec{x}_T^{i,rec} - \vec{x}_0^{i,rec}), \forall i \in \mathbb{S}, \quad (27)$$

where \mathbb{S} refers to a specific scenario, and α^{rec} is a positive scalar, which was set as 1.5 in the calibration.

For vehicle-pedestrian interaction, since all pedestrians have similar motion, the destination was estimated based on the average of all initial positions and the average of all final positions:

$$\vec{x}_t^{i,des} = \vec{x}_0^{mean,rec} + \alpha^{rec} \cdot (\vec{x}_T^{mean,rec} - \vec{x}_0^{mean,rec}), \forall i \in \mathbb{S}. \quad (28)$$

4.5 Genetic Algorithm

The GA [20] is a class of evolutionary algorithms that mimics natural selection. It is well suitable for finding the (near)-optimal solutions to complex systems. The basic operators such as mutation, crossover, and selection introduce randomness, hence possibly overcoming the local minima problem.

In the GA calibration process, Equation (1) was iteratively applied for each pedestrian to obtain simulated trajectories $\{\vec{x}_t^{i,sim}\}, \forall t \in \{1, \dots, T\}, \forall i \in \mathbb{S}$. The pedestrian's initial state was set as the initial state of the recorded trajectory $\vec{x}_0^{i,sim} := \vec{x}_0^{i,rec}, \forall i \in \mathbb{S}$, whereas vehicle applied the whole recorded trajectory $\vec{x}_t^v := \vec{x}_t^{v,rec}, \forall t \in \{0, 1, \dots, T-1\}$.

The performance of a particular parameter set Θ was evaluated by a loss function comparing the simulated trajectories to the recorded trajectories.

4.5.1 Loss Function. A classical way of designing loss function is to maximize the likelihood of every point on the pedestrian trajectory. The assumption is that the error between the simulated trajectory and the recorded trajectory is Gaussian. If the log-likelihood is maximized, as presented in Daamen and Hoogendoorn [5], it is equivalent to minimizing the mean square error:

$$\sigma_i^2(\Theta) = \frac{1}{T} \sum_{t=1}^T (\vec{x}_t^{i,rec} - \vec{x}_t^{i,sim})^2, \quad (29)$$

where Θ stands for the parameter set. This study applied mean square error as the loss (fitness) function of the GA.

4.5.2 Initialization. The parameters were initialized as the manually calibrated parameters in the previous step. Lower bounds and upper bounds were added to ensure that in the process of calibration, the parameters do not go beyond unrealistic values. For example, some parameters representing force magnitude should always be positive. And a parameter of the field of view obviously has an angle limit. The total number of population in the GA was set to 200, which is sufficient for the calibration.

4.5.3 Implementation. The calibration and evaluation were conducted in MATLAB R2018b with Simulink. The Global Optimization Toolbox is used for executing the GA. As an example of computation time, a typical GA calibration with 25 generations requires approximately 12 hours on an Intel Core i7-4790 CPU @3.60 GHz desktop computer. Simulation is done at the time interval of $\Delta t = 0.0334s$, which is equivalent to 29.97 frames per second, the same value as the frames per second in the trajectory dataset.

5 RESULT

5.1 Pedestrian-Pedestrian Interaction

In this step, only Ped2Ped parameters, as shown in Table 2, were calibrated. Some parameters that were manually calibrated in the previous step were fixed during the GA calibration. Specifically, λ^{rep} and λ^{nav} were fixed, because we believe the associated anisotropies were good enough, and the fixation could also reduce the uncertainty of running the GA calibration. σ^{des} was fixed because it only reduces the desired velocity when a pedestrian is close to his or her destination, which does not affect the pedestrian motion too much if the pedestrian has not reached the destination.

5.1.1 Calibration. The GA calibration was executed for more than 30 generations. After 20 generations, both the best fitness and the mean fitness converged. The best fitness value of 1.00468 was obtained, which means the average error of all positions in all trajectories of all pedestrians is about 1 m. This indicates the parameters were calibrated to some extent so that the model achieved its best performance based on the applied trajectory data. The obtained values of Ped2Ped parameters are presented in Table 2.

5.1.2 Validation. The validation was done by simulating pedestrians with the same initial conditions as in the data used for calibration. This allows us to compare and analyze the simulated trajectories to recorded trajectories. Figure 10 plots both types of trajectories, as well as the evolution of velocities of all pedestrians from a selected pedestrian-pedestrian interaction scenario. The blue asterisks show the initial positions of all pedestrians. The red solid lines indicate the simulated trajectories, whereas the blue dashed lines indicate recorded ground truth trajectories. The results of more scenarios can be found in Section A.1 of the supplementary materials. The trajectory plotting shows that in general, pedestrians are able to navigate around each other when

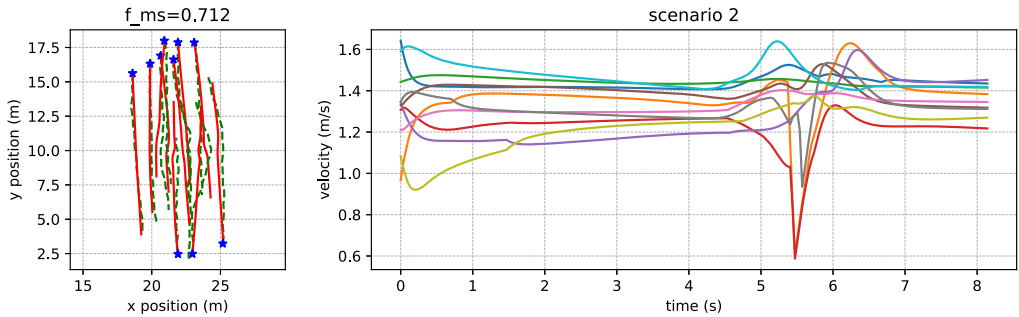


Fig. 10. Validation of a selected scenario of pedestrian-pedestrian interaction. Left: A comparison between simulated trajectories (red solid lines) and recorded trajectories (green dashed lines). The asterisks indicate the initial positions of each pedestrian. f_{ms} shown in the title is the average of the mean square errors (as defined in Equation (29)) of all pedestrians. Right: The evolution of velocities of all pedestrians in this scenario. More results can be found in Section A.1 of the supplementary materials.

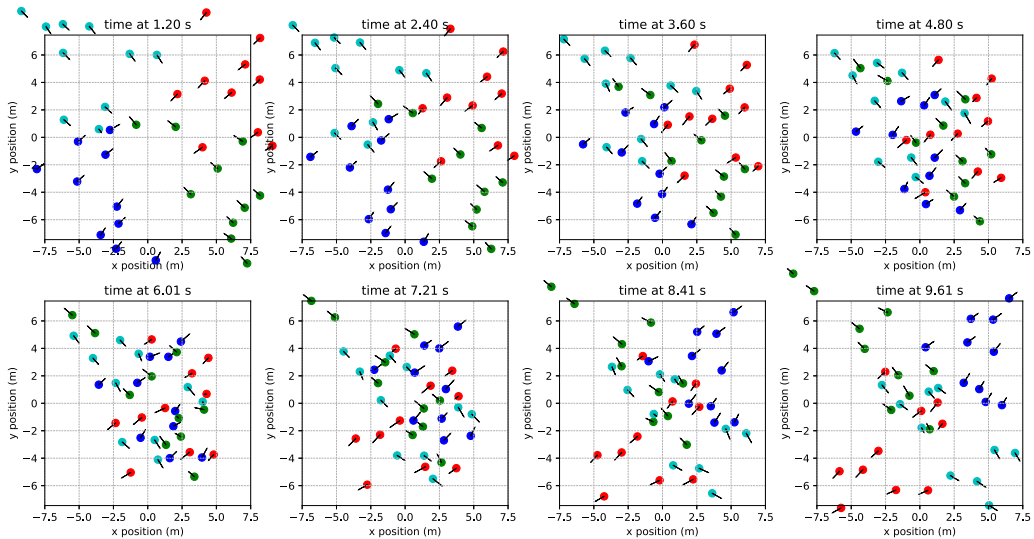


Fig. 11. Simulation of four groups of pedestrians interacting from four different directions. Pedestrians in different groups are plotted in different colors. The small black arrows indicate the walking directions and the walking velocities (length of the arrow). Different groups were randomly initialized in different quadrants and were assigned a destination in the diagonal position, respectively. For example, the red group was initialized within the area of $x \in [0, 10]$ and $y \in [0, 10]$, and assigned a destination at $[-10, -10]$.

there is potential conflict. The velocities demonstrate that pedestrians adjust their walking speed (slow down or accelerate) when interacting with each other.

5.1.3 *Post-Simulation.* Post-simulations of pedestrians in more complex scenarios were conducted to further evaluate the model based on the calibrated parameters. In particular, a scenario was designed such that four groups of pedestrians interact with each other from four different directions. The screenshots of the simulation are displayed in Figure 11. As the screenshots show (see the caption for a detailed description), all pedestrians were interacting as expected, even in the extremely dense situation. Figure 12 shows the trajectories and the evolution of velocities of all

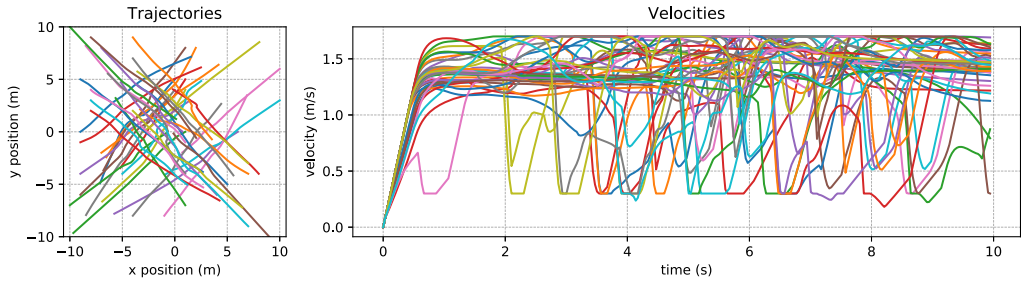


Fig. 12. Trajectories and velocities of four-group interaction. Left: Trajectories of all pedestrians in the simulation. Right: The evolution of velocities of all pedestrians in the simulation.

pedestrians in the simulation. The curved trajectories indicate the pedestrians navigate around to avoid potential collision. The multiple decreases in velocities indicate the pedestrians slow down to avoid collision.

It can be seen from the simulated pedestrian motion that each pedestrian is capable of navigating around any potential conflict with others.

5.2 Vehicle-Pedestrian Interaction

After obtaining the Ped2Ped parameters, the Veh2Ped parameters, as shown in Table 2, were calibrated by using the data that include vehicles. This step did not change the values of Ped2Ped parameters.

5.2.1 Calibration. The GA calibration was executed for more than 30 generations. Similarly, after about 20 generations, both the best fitness and the mean fitness converged. The best fitness value of 4.1918 was obtained. The obtained parameter values are shown in Table 2. The best fitness value for Veh2Ped parameters is larger compared to the best fitness value obtained for Ped2Ped parameters. This is because the vehicle-pedestrian interaction is much more complex than the pedestrian-pedestrian interaction, so it is reasonable that the fitness value is larger. Complex interaction may require a considerably large amount of data for calibration. But in any case, the convergence of both mean fitness and best fitness indicates that the model achieved its best performance based on the calibration data. Therefore, we can still conclude that the model performance was improved to some extent.

5.2.2 Validation. The model was still calibrated by simulating pedestrians with the same initial conditions as in the data used for calibration. Different from pedestrian-pedestrian interaction, vehicle motion was added in the simulation by using the ground truth vehicle trajectories. Figures 13, 14, and 15 show three selected scenarios, which correspond to back interaction, front interaction, and lateral interaction, respectively. More results can be found in Section A.2 of the supplementary materials. According to the simulated trajectories, pedestrians are able to avoid the vehicle from different directions. The velocities indicate that pedestrians may slow down or accelerate to avoid a potential collision with the vehicle. There remains a certain degree of error between the simulated trajectories and recorded trajectories, which can be explained by the following reasons:

- Different types of fundamental interactions (back, front, and lateral interactions) may need a different parameter set, which implies that one general model may not be sufficient to describe the vehicle-pedestrian interaction.

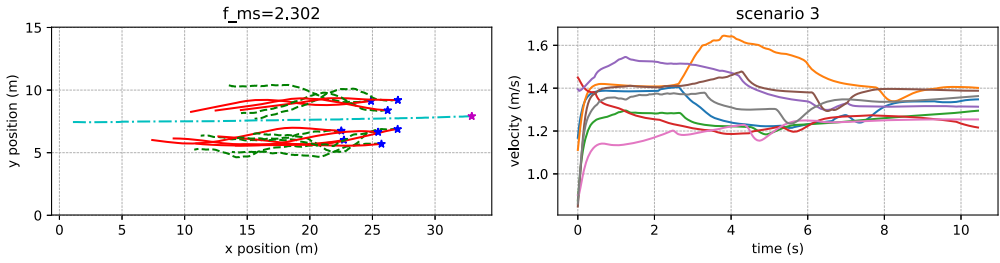


Fig. 13. Validation result of a selected scenario of back interaction. Left: A comparison between simulated trajectories (red solid lines) and recorded trajectories (green dashed lines). The cyan dash-dotted line represents the ground truth trajectory of the vehicle motion. The asterisks indicate the initial positions of each participant. f_{ms} shown in the title is the average of the mean square errors (as defined in Equation (29)) of all pedestrians. Right: The evolution of velocities of all pedestrians in this scenario. More results can be found in Section A.1 of the supplementary materials.

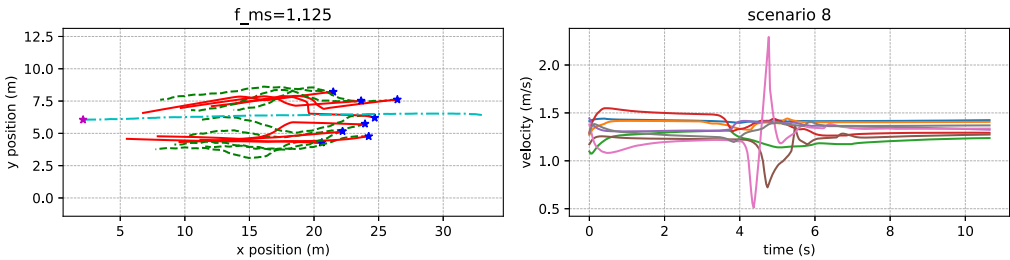


Fig. 14. Validation result of a selected scenario of front interaction. The notation is the same as in Figure 13.

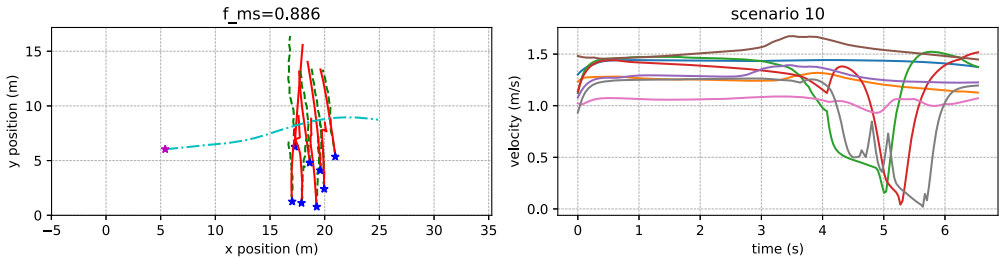


Fig. 15. Validation result of a selected scenario of lateral interaction. The notation is the same as in Figure 13.

- Our assumption of homogeneous pedestrians (every pedestrian applies the same parameter set) limits the model performance. Even for the same pedestrian in the same situation, the pedestrian behavior could also be affected by his or her inner thought (e.g., in a rush or not).
- The limited amount of data for calibration could also cause the error.

5.2.3 *Post-Simulation.* Post-simulations were conducted to further evaluate the performance of the model. Scenarios of three types of fundamental vehicle-pedestrian interactions were designed and simulated: back interaction, front interaction, and lateral interaction. The vehicle motion was simulated by using a pure pursuit controller tracking a pre-defined path, as described in Section 3.7. The simulation results are shown in Figures 16, 17, and 18, respectively. Details of the simulation configuration can be found in the figure legends. The pedestrians in the simulation are able to avoid the collision with the vehicle from different directions. Notice that in a relatively crowded

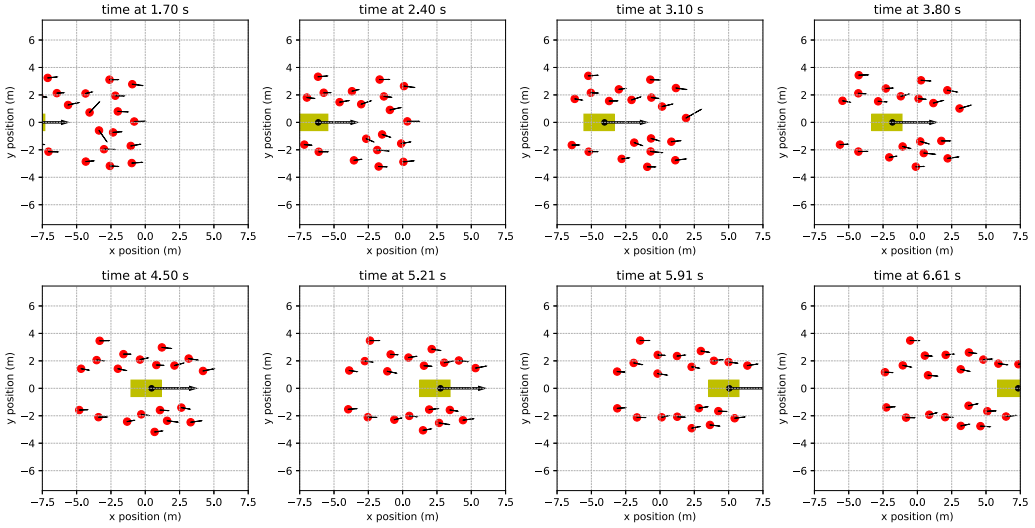


Fig. 16. Simulation snapshots of back interaction. A slowing-moving (3 m/s, which is the average speed in the dataset) vehicle (yellow box) was moving from the negative x -axis to the positive x -axis. Pedestrians (red circles) were randomly initialized within the area of $x \in [-9, -3]$ and $y \in [-3, 3]$, and assigned a destination at $[20, 0]$. The small black arrows indicate the walking directions and the walking velocities (length of the arrow) of pedestrians, whereas similarly the big black arrow indicates the orientation and the velocity of the vehicle.

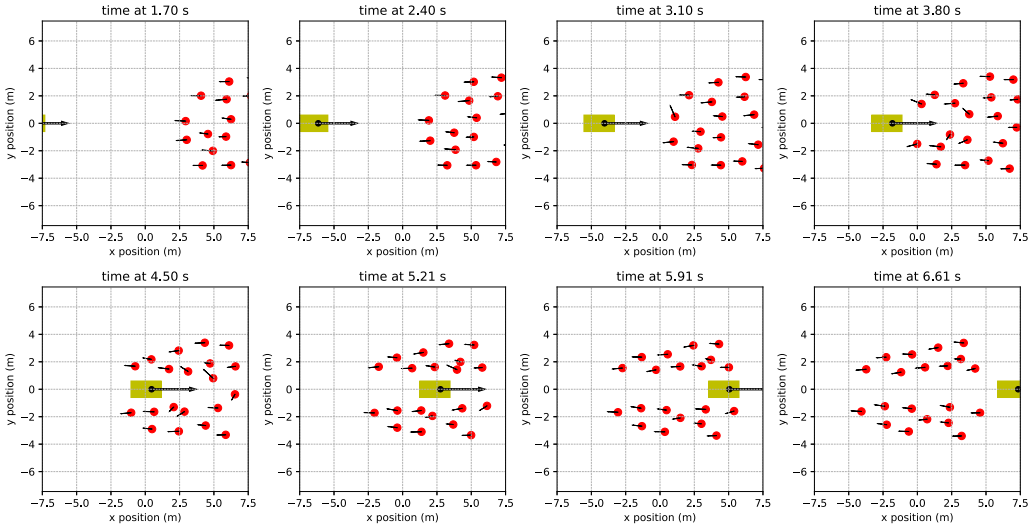


Fig. 17. Simulation snapshots of front interaction. The configuration is the same as in Figure 16, except the pedestrians were initialized within $x \in [5, 11]$ and $y \in [-3, 3]$, and assigned a destination at $[-20, 0]$.

situation, as shown in Figure 18, there are a couple of instances of small overlap among pedestrians. This is exactly what we expected because the pedestrians should be able to push others if a vehicle is approaching in a dangerous way. Trajectories and velocities of the preceding simulation can be found in Section A.3 of the supplementary materials, in which pedestrian behavior such as slowing down and accelerating to avoid the vehicle can be identified.

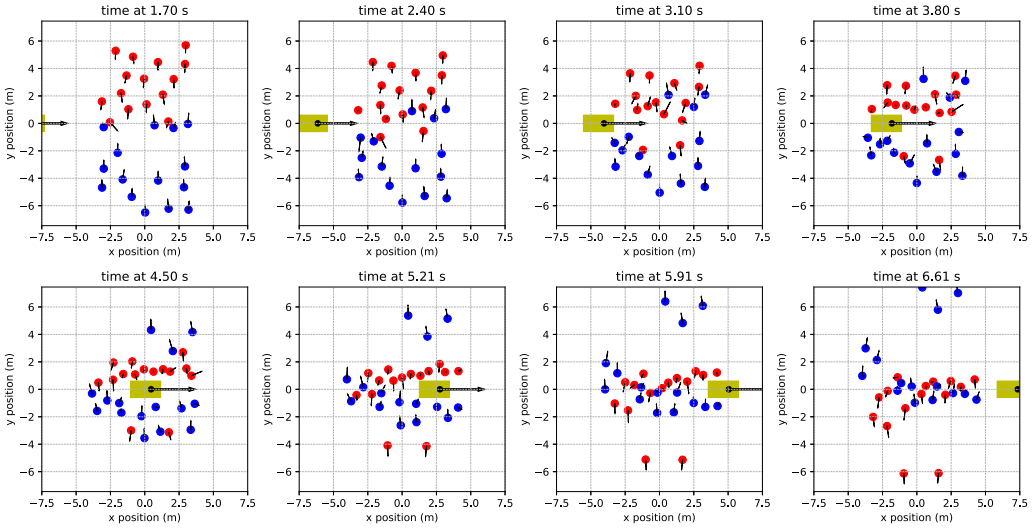


Fig. 18. Simulation snapshots of lateral interaction. The configuration is the same as in Figure 16, except there were two groups of pedestrians. One group (red circles) was initialized within $x \in [-3, 3]$ and $y \in [2, 8]$ with a destination at $[0, -20]$. The other group (blue circles) was initialized within $x \in [-3, 3]$ and $y \in [-8, -2]$ with a destination at $[0, 20]$.

Overall, although the calibration of vehicle-pedestrian interaction did not generate a very good fitness value, the post-simulation still validated the performance of the proposed model.

6 CONCLUSION

This study proposed a straightforward yet efficient social force based model that can describe the pedestrian motion under vehicle influence. The proposed model was evaluated and validated by both the simulation and calibration of fundamental vehicle-pedestrian interaction scenarios (back, front, and side interaction).

In this work, each pedestrian is assumed to be associated with a homogeneous pedestrian motion model (same values of parameters), because we were looking for a general model that can describe general pedestrian motion under vehicle influence. The proposed model is able to describe pedestrian motion in fundamental vehicle-pedestrian interaction scenarios, as demonstrated in the simulation. Pedestrian-pedestrian interaction is generally good. However, a certain amount of error exists in vehicle-pedestrian interaction, hence indicating that a homogeneous model is not enough for describing detailed pedestrian behavior under vehicle influence.

To further improve the pedestrian motion model, there are several points to consider:

- The assumption of homogeneity could be removed, and hence the pedestrian motion model can describe different types of interactions. For example, pedestrians could have different radii, different action capabilities (fast or slow), and different preferences of avoiding the collision. This can be achieved by individually calibrating a parameter set for each pedestrian or clustering a certain number of features based on the individually obtained parameters.
- The utilization of mean square error for calibration may not be a perfect choice. As the simulation timestep increases, the error accumulates. The final prediction error (the difference between the last simulated position and the last recorded position) could be considered together with the mean square error.

- Instead of using the whole pedestrian trajectory in the data for calibration, a fixed-time length trajectory can be applied. This will avoid larger cumulative error in longer trajectories.
- Different fundamental vehicle-pedestrian interaction scenarios (front, back, and lateral) may require different designs of vehicle influence, or at least different parameter sets for vehicle influence. That means the calibration of vehicle-pedestrian could be done separately.

The dataset used in this work also has some limitations:

- There is no much variation of the vehicle speed in the dataset. Our data has an average vehicle speed of 3 m/s. Whether the proposed model generalizes to the influence of the vehicle of higher speed has not been validated by the data. The dataset with different vehicle velocities is desirable.
- Pedestrian participants in our dataset do not represent all kinds of pedestrians, since they are primarily composed of college students. In addition, the density of the pedestrian crowd does not vary too much.

Therefore, more datasets with a variety of vehicle-pedestrian interaction patterns are eagerly desired. Fortunately, there a better dataset has been available, the DUT dataset in Yang et al. [32], which consists of natural vehicle-pedestrian interaction on a university campus. Calibrating the proposed model based on the new dataset will be our next step.

Regarding multi-modality, various types of road users (e.g., cyclists, animals) should be considered in the future to make the pedestrian motion model more generalizable. But still, among these road users, vehicles should be the primary concern, as they are the most dominant and dangerous participants in the traffic.

A SUPPLEMENTARY MATERIALS

A.1 Validation of Pedestrian-Pedestrian Interaction

Figure 19 shows the validation results of all scenarios of pedestrian-pedestrian interaction.

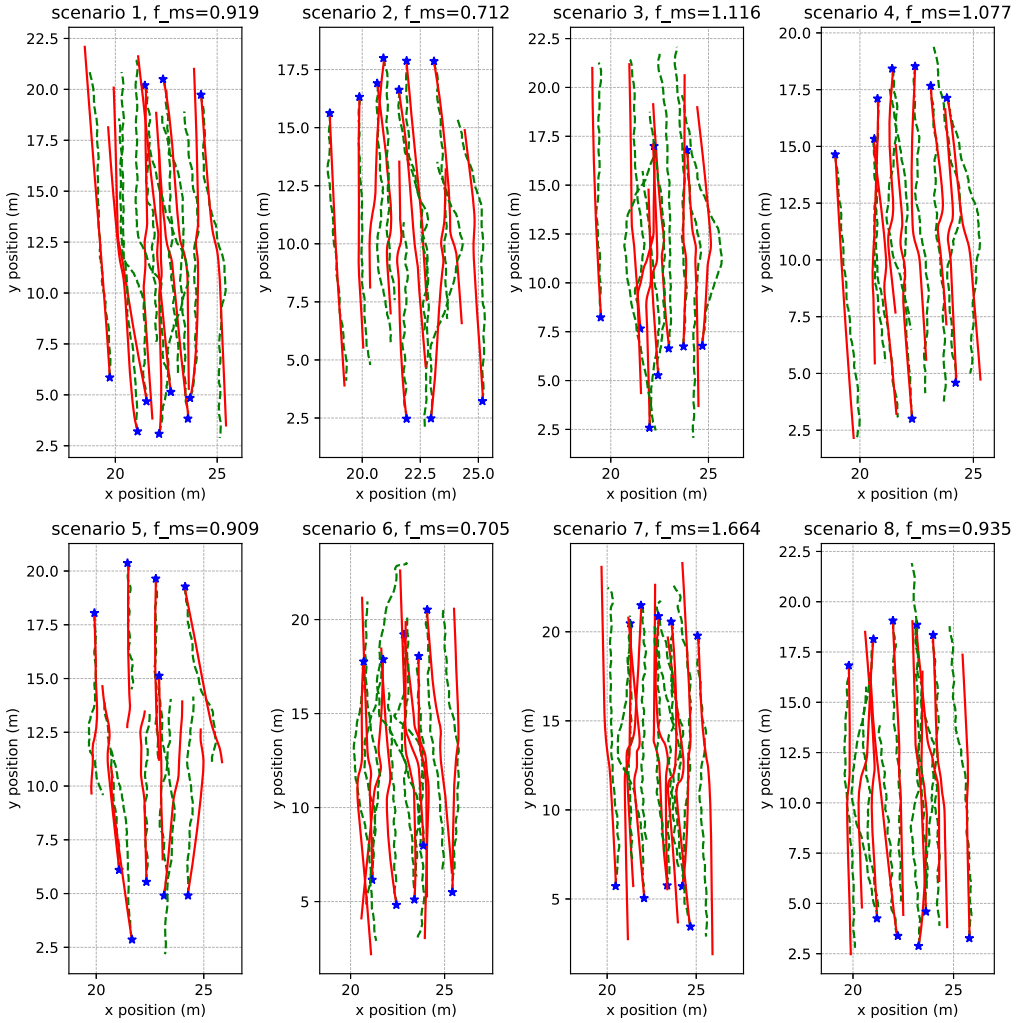


Fig. 19. A comparison between simulated trajectories (red solid lines) and recorded trajectories (green dashed lines) in pedestrian-pedestrian interaction scenarios. f_{ms} shown in the title is the average of the mean square errors (as defined in Equation (29)) of all pedestrians in the scenario. The asterisks indicate the initial positions of each pedestrian.

A.2 Validation of Vehicle-Pedestrian Interaction

Figure 20 shows the validation results of all scenarios of vehicle-pedestrian interaction.

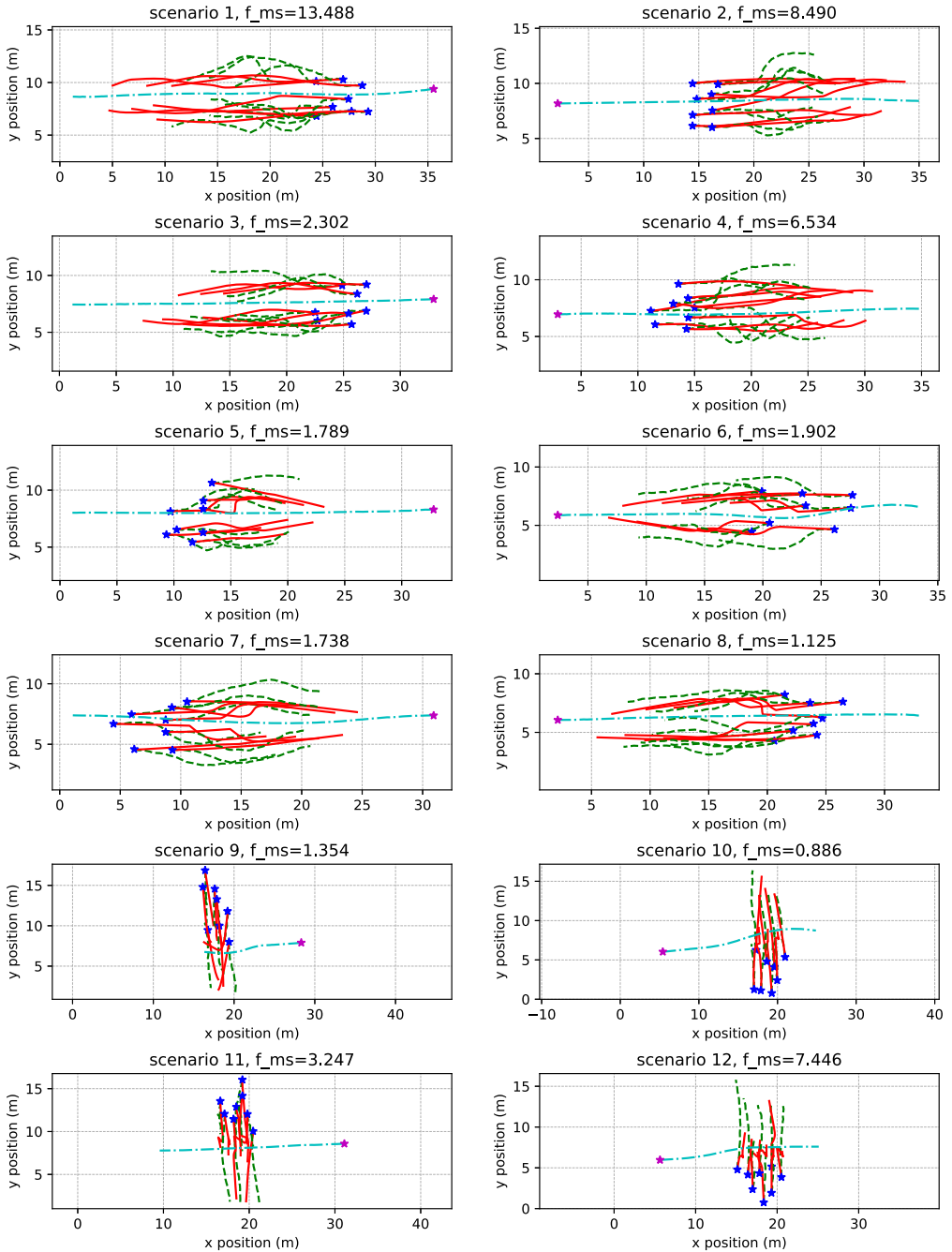


Fig. 20. A comparison between simulated trajectories (red) and recorded trajectories (black) of pedestrians in vehicle-pedestrian interaction scenarios (i.e., scenarios that consider vehicle influence). f_{ms} is the mean square error as defined in Equation (29). The vehicle motion uses ground truth, of which the trajectories are indicated in dash-dotted cyan. The asterisks indicate initial positions. Rows 1-2, 3-4, and 5-6 show scenarios of back interaction, front interaction, and lateral interaction, respectively.

A.3 Post-Simulation of Vehicle-Pedestrian Interaction

Figures 21, 22, and 23 show the trajectories and velocities of back, front, and lateral interactions that correspond to Figures 16, 17, and 18, respectively, in the post-simulation.

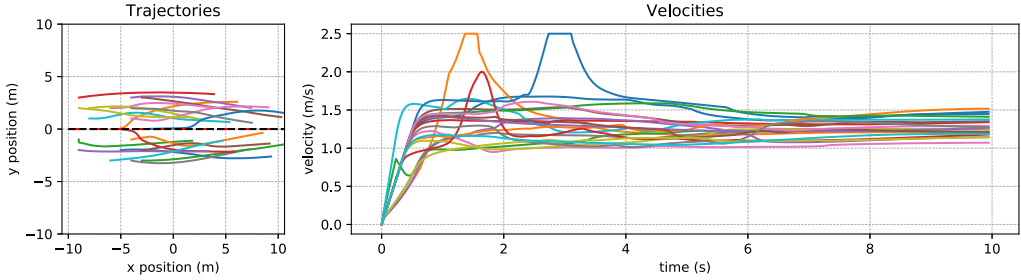


Fig. 21. Trajectories and velocities of back interaction. Left: Trajectories of pedestrians (solid lines) and the vehicle (dashed line) in the simulation. Right: The evolution of velocities of all pedestrians in the simulation.

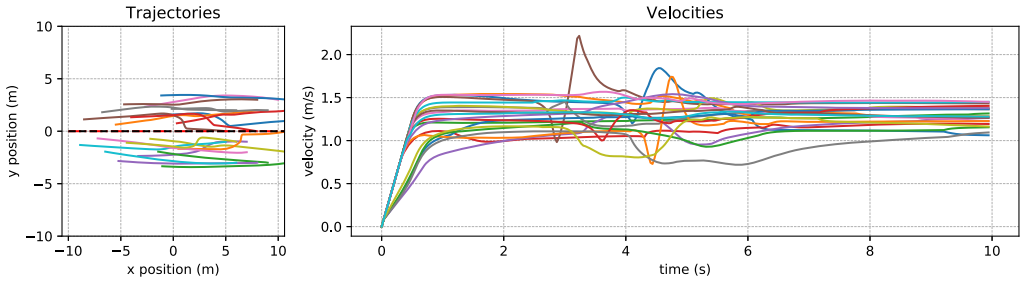


Fig. 22. Trajectories and velocities of front interaction. Left: Trajectories of pedestrians (solid lines) and the vehicle (dashed line) in the simulation. Right: The evolution of velocities of all pedestrians in the simulation.

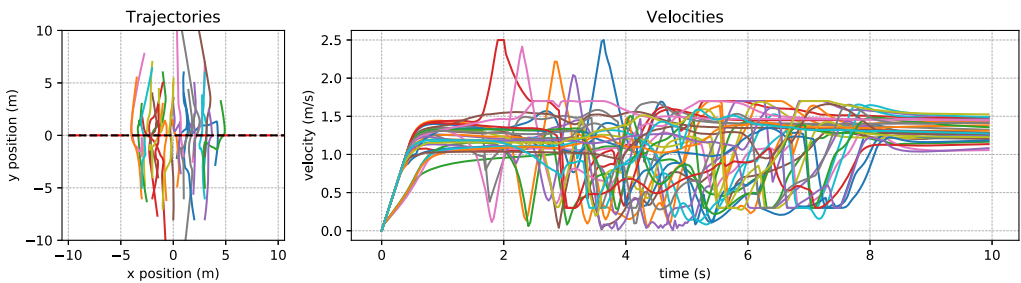


Fig. 23. Trajectories and velocities of lateral interaction. Left: Trajectories of pedestrians (solid lines) and the vehicle (dashed line) in the simulation. Right: The evolution of velocities of all pedestrians in the simulation.

REFERENCES

- [1] Alexandre Alahi, Kratharth Goel, Vignesh Ramanathan, Alexandre Robicquet, Li Fei-Fei, and Silvio Savarese. 2016. Social LSTM: Human trajectory prediction in crowded spaces. In *Proceedings of the IEEE Conference on Computer Vision and Pattern Recognition*. 961–971.
- [2] Gianluca Antonini, Michel Bierlaire, and Mats Weber. 2006. Discrete choice models of pedestrian walking behavior. *Transportation Research Part B: Methodological* 40, 8 (2006), 667–687.

- [3] Bani Anvari, Michael G. H. Bell, Aruna Sivakumar, and Washington Y. Ochieng. 2015. Modelling shared space users via rule-based social force model. *Transportation Research Part C: Emerging Technologies* 51 (2015), 83–103.
- [4] Gabriele Bernardini, Enrico Quagliarini, and D’Orazio. 2016. Towards creating a combined database for earthquake pedestrians’ evacuation models. *Safety Science* 82 (2016), 77–94.
- [5] Winnie Daamen and Serge Hoogendoorn. 2012. Calibration of pedestrian simulation model for emergency doors by pedestrian type. *Transportation Research Record* 2316, 1 (2012), 69–75.
- [6] Rayan El Helou. 2016. *Agent-Based Modelling of Pedestrian Microscopic Interactions*. Master’s Thesis. Ohio State University.
- [7] Claudio Feliciani, Luca Crociani, Andrea Gorrini, Giuseppe Vizzari, Stefania Bandini, and Katsuhiro Nishinari. 2017. A simulation model for non-signalized pedestrian crosswalks based on evidence from on field observation. *Intelligenza Artificiale* 11, 2 (2017), 117–138.
- [8] Andrea Gorrini, Luca Crociani, Giuseppe Vizzari, and Stefania Bandini. 2018. Observation results on pedestrian-vehicle interactions at non-signalized intersections towards simulation. *Transportation Research Part F: Traffic Psychology and Behaviour* 59 (2018), 269–285.
- [9] Agrim Gupta, Justin Johnson, Li Fei-Fei, Silvio Savarese, and Alexandre Alahi. 2018. Social GAN: Socially acceptable trajectories with generative adversarial networks. In *Proceedings of the IEEE Conference on Computer Vision and Pattern Recognition*. 2255–2264.
- [10] Shlomi Hacohen, Nir Shvalb, and Shraga Shoval. 2018. Dynamic model for pedestrian crossing in congested traffic based on probabilistic navigation function. *Transportation Research Part C: Emerging Technologies* 86 (2018), 78–96.
- [11] Dirk Helbing, Illés Farkas, and Tamas Vicsek. 2000. Simulating dynamical features of escape panic. *Nature* 407, 6803 (2000), 487.
- [12] Dirk Helbing and Peter Molnar. 1995. Social force model for pedestrian dynamics. *Physical Review E* 51, 5 (1995), 4282.
- [13] Serge P. Hoogendoorn and Piet H. L. Bovy. 2004. Pedestrian route-choice and activity scheduling theory and models. *Transportation Research Part B: Methodological* 38, 2 (2004), 169–190.
- [14] Anders Johansson, Dirk Helbing, and Pradyumn K. Shukla. 2007. Specification of the social force pedestrian model by evolutionary adjustment to video tracking data. *Advances in Complex Systems* 10, supp02 (2007), 271–288.
- [15] Fatema T. Johora and Jörg P. Müller. 2018. Modeling interactions of multimodal road users in shared spaces. In *Proceedings of the 2018 21st International Conference on Intelligent Transportation Systems (ITSC’18)*. IEEE, Los Alamitos, CA, 3568–3574.
- [16] Yoshiaki Kuwata, Justin Teo, Sertac Karaman, Gaston Fiore, Emilio Frazzoli, and Jonathan P. How. 2008. Motion planning in complex environments using closed-loop prediction. In *Proceedings of the AIAA Guidance, Navigation, and Control Conference and Exhibition*.
- [17] Alon Lerner, Yiorgos Chrysanthou, and Dani Lischinski. 2007. Crowds by example. *Computer Graphics Forum* 26, 3, 655–664.
- [18] Robert V. Levine and Ara Norenzayan. 1999. The pace of life in 31 countries. *Journal of Cross-Cultural Psychology* 30, 2 (1999), 178–205.
- [19] Peng Lin, Jian Ma, and Siuming Lo. 2016. Discrete element crowd model for pedestrian evacuation through an exit. *Chinese Physics B* 25, 3 (2016), 034501.
- [20] Melanie Mitchell. 1998. *An Introduction to Genetic Algorithms*. MIT Press, Cambridge, MA.
- [21] Betty J. Mohler, William B. Thompson, Sarah H. Creem-Regehr, Herbert L. Pick, and William H. Warren. 2007. Visual flow influences gait transition speed and preferred walking speed. *Experimental Brain Research* 181, 2 (2007), 221–228.
- [22] Mehdi Moussaïd, Dirk Helbing, and Guy Theraulaz. 2011. How simple rules determine pedestrian behavior and crowd disasters. *Proceedings of the National Academy of Sciences* 108, 17 (2011), 6884–6888.
- [23] Umit Ozguner, Tankut Acarman, and Keith Alan Redmill. 2011. *Autonomous Ground Vehicles*. Artech House.
- [24] F. Pascucci, N. Rinke, C. Schiermeyer, B. Friedrich, and V. Berkhahn. 2015. Modeling of shared space with multi-modal traffic using a multi-layer social force approach. *Transportation Research Procedia* 10 (2015), 316–326.
- [25] Stefano Pellegrini, Andreas Ess, Konrad Schindler, and Luc Van Gool. 2009. You’ll never walk alone: Modeling social behavior for multi-target tracking. In *Proceedings of the 2009 IEEE 12th International Conference on Computer Vision*. IEEE, Los Alamitos, CA, 261–268.
- [26] N. Rinke, C. Schiermeyer, F. Pascucci, V. Berkhahn, and B. Friedrich. 2017. A multi-layer social force approach to model interactions in shared spaces using collision prediction. *Transportation Research Procedia* 25 (2017), 1249–1267.
- [27] Andreas Schadschneider, Wolfram Klingsch, Hubert Klüpfel, Tobias Kretz, Christian Rogsch, and Armin Seyfried. 2009. Evacuation dynamics: Empirical results, modeling and applications. In *Encyclopedia of Complexity and Systems Science*. Springer, 3142–3176.
- [28] Robert Schönauer, Martin Stubenschrott, Weinan Huang, Christian Rudloff, and Martin Fellendorf. 2012. Modeling concepts for mixed traffic: Steps toward a microscopic simulation tool for shared space zones. *Transportation Research Record* 2316, 1 (2012), 114–121.

- [29] Valeria Vignali, Federico Cuppi, Ennia Acerra, Arianna Bichicchi, Claudio Lantieri, Andrea Simone, and Marco Costa. 2019. Effects of median refuge island and flashing vertical sign on conspicuity and safety of unsignalized crosswalks. *Transportation Research Part F: Traffic Psychology and Behaviour* 60 (2019), 427–439.
- [30] Yao Xiao, Ziyu Gao, Yunchao Qu, and Xingang Li. 2016. A pedestrian flow model considering the impact of local density: Voronoi diagram based heuristics approach. *Transportation Research Part C: Emerging Technologies* 68 (2016), 566–580.
- [31] Hao Xue, Du Q. Huynh, and Mark Reynolds. 2018. SS-LSTM: A hierarchical LSTM model for pedestrian trajectory prediction. In *Proceedings of the 2018 IEEE Winter Conference on Applications of Computer Vision (WACV'18)*. IEEE, Los Alamitos, CA, 1186–1194.
- [32] Dongfang Yang, Linhui Li, Keith Redmill, and Ümit Özgüner. 2019. Top-view trajectories: A pedestrian dataset of vehicle-crowd interaction from controlled experiments and crowded campus. In *Proceedings of the 2019 IEEE Intelligent Vehicles Symposium (IV'19)*. IEEE, Los Alamitos, CA, 899–904.
- [33] Dongfang Yang, Ümit Özgüner, and Keith Redmill. 2018. Social force based microscopic modeling of vehicle-crowd interaction. In *Proceedings of the 2018 IEEE Intelligent Vehicles Symposium (IV'18)*. IEEE, Los Alamitos, CA, 1537–1542.
- [34] Francesco Zanlungo, Tetsushi Ikeda, and Takayuki Kanda. 2011. Social force model with explicit collision prediction. *EPL (Europhysics Letters)* 93, 6 (2011), 68005.
- [35] Weiliang Zeng, Peng Chen, Guizhen Yu, and Yunpeng Wang. 2017. Specification and calibration of a microscopic model for pedestrian dynamic simulation at signalized intersections: A hybrid approach. *Transportation Research Part C: Emerging Technologies* 80 (2017), 37–70.
- [36] Weiliang Zeng, Hideki Nakamura, and Peng Chen. 2014. A modified social force model for pedestrian behavior simulation at signalized crosswalks. *Procedia-Social and Behavioral Sciences* 138 (2014), 521–530.

Received December 2018; revised November 2019; accepted November 2019